minerals

MDPI

Article

Massive Sulfide Ores in the Iberian Pyrite Belt: Mineralogical and Textural Evolution

Gabriel R. Almodóvar [1], Lola Yesares [2,*], Reinaldo Sáez [1], Manuel Toscano [1], Felipe González [1] and Juan Manuel Pons [3]

[1] Departamento de Ciencias de la Tierra, Universidad de Huelva, 21071 Huelva, Spain; almodovar@uhu.es (G.R.A.); saez@uhu.es (R.S.); mtoscano@dgeo.uhu.es (M.T.); fbarrio@uhu.es (F.G.)
[2] iCRAG and School of Earth Sciences, University College Dublin, Dublin 4, Ireland
[3] MATSA SAU, Almonaster la Real, 21342 Huelva, Spain; juan.pons@matsamining.com
* Correspondence: lola.yesares@dgeo.uhu.es

Received: 10 September 2019; Accepted: 21 October 2019; Published: 24 October 2019

Abstract: The Iberian Pyrite Belt (IPB) is recognized as having one of the major concentrations of volcanogenic massive sulfide (VMS) deposits on Earth. Original resources of about 2000 Mt of massive sulfides have been reported in the province. Recent classifications have considered the IPB deposits as the bimodal siliciclastic subtype, although major differences can be recognized among them. The main ones concern the hosting rocks. To the north, volcanic and volcaniclastic depositional environments predominate, whereas to the south, black shale-hosted VMS prevail. The mineral composition is quite simple, with pyrite as the main mineral phase, and sphalerite, galena, and chalcopyrite as major components. A suite of minor minerals is also present, including arsenopyrite, tetrahedrite–tennantite, cobaltite, Sb–As–Bi sulfosalts, gold, and electrum. Common oxidized phases include magnetite, hematite, cassiterite, and barite. The spatial relationship between all these minerals provides a very rich textural framework. A careful textural analysis reported here leads to a general model for the genetic evolution of the IPB massive sulfides, including four main stages: (1) Sedimentary/diagenetic replacement process on hosting rocks; (2) sulfides recrystallization at rising temperature; (3) metal distillation and sulfides maturation related to late Sb-bearing hydrothermal fluids; and (4) metal remobilization associated with the Variscan tectonism. The proposed model can provide new tools for mineral exploration as well as for mining and metallurgy.

Keywords: VMS; textural evolution; Iberian Pyrite Belt

1. Introduction

The genetic model for volcanogenic massive sulfide (VMS) deposits has been well developed in classic papers [1–5]. In most massive sulfide genetic environments, the evolution of submarine hydrothermalism occurs at rising temperatures. These hydrothermal processes commonly occur over a protracted period of time and they persist after the deposition of massive sulfides, which promotes the generation of zones of enriched metals formed by the interaction of hydrothermal fluids with early-formed massive sulfide mineralization [1,3,6,7].

The Iberian Pyrite Belt (IPB) has been one of the major mining districts in Europe since prehistoric times [8,9]. It is an area of significant geological and metallogenic interest because it represents the largest concentration of metallic sulfide deposits on Earth [10–12]. With more than 2000 Mt of massive sulfide ore, the IPB comprises an exceptional number of supergiant deposits, including the biggest in this class: Riotinto (>500 Mt) and Neves Corvo (≥300 Mt) [13,14].

The general characteristics of the IPB sulfide deposits, including their geological context, are well-documented in the literature [10–26]. These studies mostly deal with geodynamic interpretations;

structural and tectonic settings; genetic models; the origin of mineralizing fluids; and economic aspects related to resources, reserves, tonnages, and ore grades.

In spite of the enormous amount of published research, the generation of massive sulfide deposits in the IPB remains controversial. At least a part of this issue is due to a generalized tendency to assimilate the ore genesis in the IPB to classic genetic models for VMS deposits which are based on present comparables (i.e., black smokers, brine pool). A general review of published proposals for the generation of VMS in the IPB is detailed below. Geodynamic interpretations suggest that during the Late Devonian–Mississippian the IPB was affected by a period of regional extension with the breakdown and compartmentation of Late Devonian homogeneous basin and the beginning of the volcanic activity [26,27]. This paleogeographic environment favored the generation of hydrothermal systems, and the formation of the massive sulfide deposits [10]. According to Barriga [28] and Barriga and Fyfe [29], mineralizing fluids derived from seawater were equilibrated with underlying volcanic, volcanoclastic, and sedimentary rocks. These fluids were expelled on the seafloor where massive sulfide formed below a sealing chert layer that promoted ore precipitation but inhibited oxidation and dispersion. Based on Pb isotope analyses, Marcoux et al. [30] showed a homogenized metal source. Sáez et al. [11,23,31] and Almodóvar et al. [18] proposed that this metal source was related to large volumes of both sea- and connate-water trapped in the underlaying volcanoclastic and sedimentary pile. This authors [11] proposed a hybrid model (called Iberian Type), between both sedimentary exhalative (SEDEX) and VMS deposits applies to the IPB, with subseafloor formation of sulfide deposits. In some cases, bacterial sulfate reduction (BSR) produced euxinic conditions in the marine environment, favoring the generation of mainly pyrite [31]. Velasco et al. [21] shown an increase of heavy S isotope values along with sulfides' textural evolution, suggesting two different sulfur sources for in the ore genesis. Light sulfide sulfur derived from BSR played the main role in earlier stages of MS genesis. Whereas heavier sulfur derived from hydrothermal sources promotes sulfides maturation during later stages. Tornos and Heinrich and Tornos et al. [20,32], suggested later that the Tharsis orebody was deposited in an anoxic brine pool where the Devonian sediments were the source for metals and hydrothermal fluids. Relvas et al. [14] proposed a more complex system for the Neves Corvo deposit. A metamorphic or granite related source was claimed as responsible for the cassiterite rich ore, whereas a metal source similar to that described above was proposed for the general massive sulfide deposit. Recently, Castroviejo et al. [25] and Marginac et al. [33] reported late metal remobilization and local enrichment during Variscan deformation and metamorphism.

Less attention has been paid to the ore mineralogy forming the massive sulfide deposits and its textural evolution. Nevertheless, there are a number of case studies documenting the mineralogy of single deposits [18,22,26,34–37]. The main ore mineralogy reported for the IPB deposits is pyrite, with subordinate sphalerite, galena, chalcopyrite, tetrahedrite–tennantite, arsenopyrite, pyrrhotite, and many other minor phases, such as Bi- and Pb-sulfosalts, cassiterite, magnetite, stannite, electrum and cobaltite. It is very well known that regardless of the setting and geological characteristics of the deposits, they share common mineralogical and textural characteristics. However, no studies propose an overall model for their textural and mineralogical evolution that accounts for the processes involved in the generation of the different mineralization styles recognized in the IPB.

This work aims to synthesize the mineralogical and textural features of IPB deposits independently of their location, host rocks, structural setting, tonnages and grades. The present study addresses for the first time the global mineralogical and textural features associated with the evolution of VMS mineralization within the IPB, from the earliest to the latest stages. Mineral associations and textures were analyzed in samples from several VMS deposits of the Spanish part of the IPB, revealing successive interactions between fluids and mineralization. The results and evolution model presented here are significant for VMS exploration because they explain the ore shoot formation mechanisms in dominant pyrite mineralizations.

2. Geological Context

The IPB is located in the southwest corner of the Iberian Peninsula, extending 230 km long and 40 km wide, from Seville, in Spain, to south of Lisbon, in Portugal (Figure 1). The IPB is the largest of the three domains comprising the South Portuguese Zone (SPZ), the southernmost zone in the Iberian Variscan Massif. This has been envisaged as a tectonostratigraphic terrain sutured to the Iberian Massif during Variscan times [12].

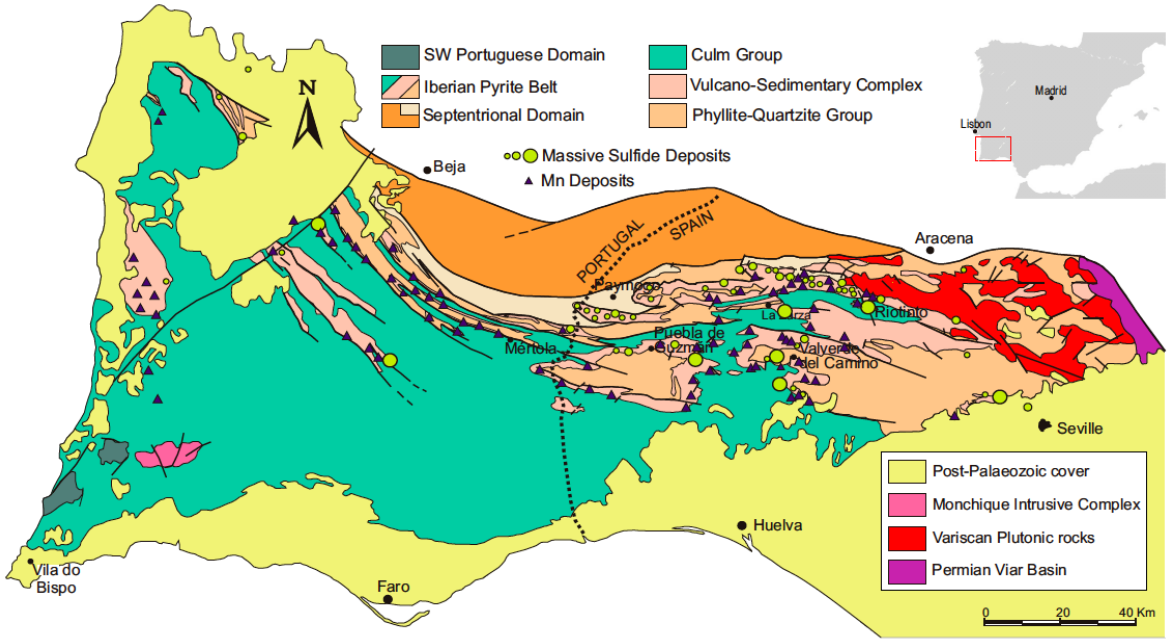

Figure 1. Geologic map of the South Portuguese Zone including the location of the most important massive sulfide deposits within the Iberian Pyrite Belt. The sketch at the top right corner indicates the location of the South Portuguese Zone within the Iberian Peninsula (modified from Sáez [38]).

The stratigraphic succession of the IPB consists of Upper Palaeozoic (Middle Devonian–Mississippian) sedimentary and igneous rocks, classically subdivided into three lithostratigraphic units. According to Schermerhörn [15] these are the Middle–Upper Devonian Phyllite–Quartzite Group (PQ Group), the Upper Devonian–Mississippian Volcano–Sedimentary Complex (VSC) and the Mississippian post-volcanic succession (Culm Group). The limits of the three units are depositional, although they appear locally tectonized.

GGeodynamic interpretations suggest that the IPB was affected by extensional tectonic processes during the Late Devonian–Mississippian transtensional phase [24]. Such regime was responsible for the breakdown and compartmentation of the basin and the onset of volcanism [27]. This paleogeographic scenario favored the generation of anoxic sub-basins where massive sulfides accumulated [10]. The episodic ascent of magma, just below the segmented basin, could have triggered the establishment of a hydrothermal system. Large volumes of seawater with connate water trapped in the volcanic and sedimentary pile may have been the source of the fluids necessary for the transport and deposition of metals [29].

It is commonly accepted that massive sulfide deposits in the IPB were deposited between the late Famennian and early Visean [23,39–42].

The IPB was intensely deformed during the Variscan orogeny. The Variscan deformation was polyphasic, involving three main stages. The first stage, late Bashkirian–early Moscovian [15], produced the major regional structures and was responsible for the thin-skinned deformation with S-verging asymmetric folds and thrusts. The second stage gently folded the main F1 foliation, with vertical,

north–south axial planes. The third deformation stage resulted in several fault systems, which modified locally the structure of the massive sulfides [43,44].

3. Samples and Methods

The work presented here summarizes the knowledge acquired during more than 30 years studying the ore mineralogy and textures of the most relevant massive sulfide deposits in the Spanish part of the IPB. This knowledge was attained throughout a number of scientific projects and transference contracts with all the mining companies that operated in the IBP during the last decades. The geology, geochemistry, mineralogy and textures were studied in about 800 samples from Tharsis, Las Cruces, Magdalena, Cueva de la Mora, Aguas Teñidas, San Miguel, Aznalcollar, Massa Valverde, Frailes, Masa Valverde, Riotinto, Sierrecilla, El Carmen, Herrerías, Sotiel Coronada, Migollas, Concepción and Castillo de Buitron, among others.

This work includes mineralogical and textural results from Magdalena, Cueva de la Mora, Aguas Teñidas, San Miguel, Aznalcóllar, Massa Valverde and Frailes, although similar features have also been observed in other IPB deposits not included here. Mineralogical and textural characterization were undertaken by optical microscope. Detailed mineralogical studies were carried out by both a JEOL scanning electron microscope coupled with energy dispersive spectroscopy (JMS-5410) and equipped with a microanalyzer Link Oxford; and a Fei-QUANTA 200 equipped with a microanalyzer EDAX Genesis 2000 from the University of Huelva, Huelva, Spain.

4. Orebody Morphology and Relationship with Hosting Rocks

The IPB orebodies correlate with the classic VMS-type model. This includes a stratabound tabular to lenticular massive upper lens and an underlying pervasive veining and sulfide dissemination forming the stockwork mineralizations. Major mine districts consist of several massive orebodies, often interconnected (e.g., Neves Corvo, Riotinto, and Tharsis [31]).

The IPB sulfide deposits are hosted by the VSC, a unit formed by a wide range of sedimentary, volcanic, volcaniclastic, and hydrothermal rocks [10–12,15,45]. The most common hosting lithologies are felsic volcanic and volcaniclastic rocks in the northern part (e.g., Aguas Teñidas, Magdalena, Cueva de la Mora and San Miguel) and black shales to the south (e.g., Aznalcóllar, Frailes and Massa Valverde) (Figure 2).

The geometric relationships between host rocks and mineralizations are mostly related to replacement (Figure 2). Replacement of volcanoclastic rocks occurs preferentially through porous levels in Aguas Teñidas, Magdalena and San Miguel (Figure 2a), while replacement of black shales takes place when the sediments were still unconsolidated in Cueva de la Mora, Aznalcóllar, Frailes and Massa Valverde [31] (Figure 2b). These suggest, also according with other authors [16,18,31,46], that at least part of the mineralization process occurs by replacement beneath the seafloor.

The occurrence of silica caps at the hanging wall of many deposits is also common in the massive sulfide deposits [28]. In the IPB, silica cap was identified in Magdalena, Aljustrel [16,29] and Tharsis [20,31]. Leistel et al. [47], deal with the relationships between silica levels and massive sulfide lenses, addressing the existence of silica caps on several deposits. That paper includes stratigraphic columns with representative massive sulfide and silica levels. Tornos [48] also account for this issue. Analogies between recent and ancient IPB silica caps suggest a comparable origin [28,29,31]. This includes silica dissolution by ascending hot fluids during early hydrothermal stages and later precipitation, at cooler temperatures, when the Si-enriched fluid mixes with both connate and sea water [1,3,7,29].

Aguas Teñidas and Magdalena also include late mafic igneous rocks emplaced in the vicinity of the orebodies before the Variscan folding. The increased temperature during the emplacement of theses late mafic rocks [49] could have derived from the recrystallization of sulfide minerals and, eventually, the reactivation of the hydrothermal systems, leading to local enrichment of ore metals.

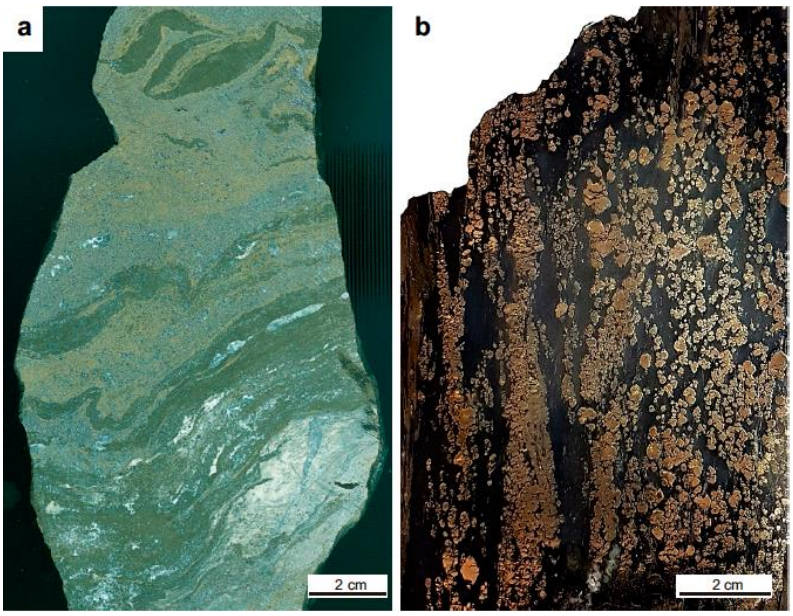

Figure 2. Massive sulfides generated by replacement of: (**a**) volcaniclastic rocks replaced by polymetallic sulfides, from Aguas Teñidas, showing of dacitic volcanic rocks embedded and corroded by sulfides. The banded facies show an original slumping fold, including very thin bands of sedimentary pyrite bearing shale. Coarse sized bands correspond to porous volcaniclastic beds pervasively replaced by sulfides (i.e.,: Galena, sphalerite, pyrite and chalcopyrite) and carbonates; and (**b**) black shales from Cueva de la Mora, where pyrite aggregates pervasively replace the rock.

5. Ore Mineralogy and Textures

The IPB sulfide deposits have a simple composition in terms of main mineralogy. By contrast, the minor mineralogy and the textural relationships are particularly complex. These are explained by an ongoing spatial–temporal variation caused by recrystallization, overgrowth, fracturation, remobilization, and replacement processes from low- to high-temperature mineral associations. These result in the generation of several mineralization styles, each one showing a distinctive mineralogical composition.

5.1. Magnetite Mineralization

Magnetite lenses were identified in some of the volcanic rock-hosted VMS deposits of the northern IPB, including Aguas Teñidas, Magdalena, San Miguel, Cueva de la Mora, Massa Valverde and Frailes. These commonly occur in the footwall of the stratiform orebodies and at the hanging wall of stockworks (e.g., including Aguas Teñidas, Magdalena, San Miguel and Cueva de la Mora), whereas in some minor cases, magnetite occurs at the hanging wall of massive sulfides (e.g., Massa Valverde and Frailes). It mostly consists of a massive concentration of idiomorphic to sub-idiomorphic magnetite crystals. Magnetite is frequently corroded and replaced by pyrite in pyritic mineralizations at Aguas Teñidas and San Miguel deposits (Figure 3a–c). Magnetite was also observed to be replaced by sphalerite in polymetallic mineralization at the Magdalena deposit (Figure 3d). Tabular magnetite crystals were also observed as hematite pseudomorphs (Figure 3a).

5.2. Barite Mineralization

Barite was identified in some volcanic rock-hosted deposits of the northern IPB, such as Aguas Teñidas and Magdalena. The textual analysis indicates that barite is an early phase within the hydrothermal system. It shows textures including corroded edges and overgrowths of colloform pyrite (Figure 4a); tabular crystals corroded and replaced by major sulfides (Figure 4b); and tabular barite crystals exhibiting pyrite rims (Figure 4c) and possible replaced by sphalerite (Figure 4d).

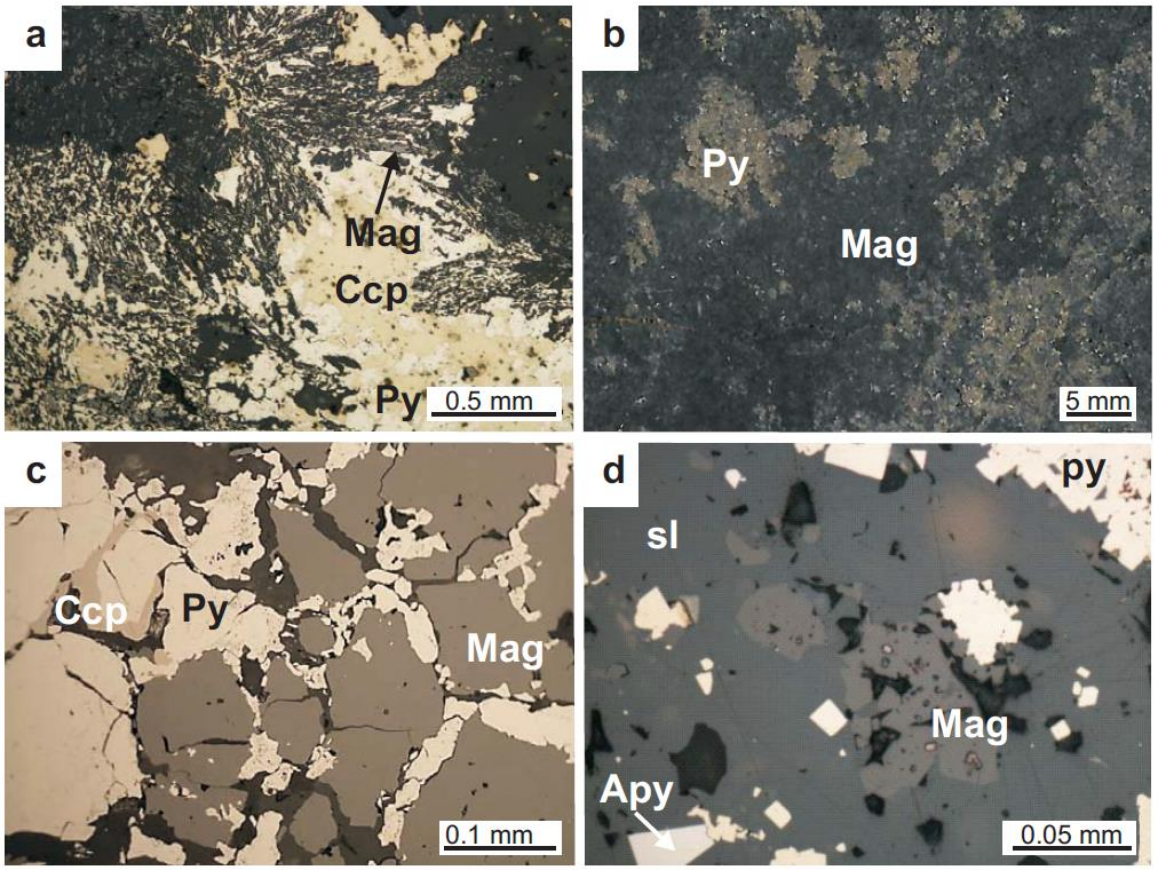

Figure 3. Optical microscope images of magnetite mineralization from several massive sulfide deposits of the IPB. (**a**) Relicts of radial magnetite (Mag) aggregates partially replaced by pyrite (Py). Chalcopyrite filling interstices in pyrite aggregates is also observed; (**b**) massive magnetite partially replaced by xenomorphic pyritic aggregates; (**c**) magnetite showing mosaic texture partially replaced by pyrite along intergranular spaces. In addition, pyrite is replaced by chalcopyrite; (**d**) subidiomorphic magnetite crystals partially corroded and embedded in sphalerite (Sp). Sphalerite is associated with idiomorphic pyrite and arsenopyrite (Apy) grains. Aguas Teñidas deposit (**a**,**c**); Magdalena deposit (**b**); San Miguel deposit (**d**).

5.3. Pyrite Mineralization

Pyrite is the most abundant mineral in the IPB sulfide deposits. Pyrite mineralization was identified in all the deposits studied from the northern and southern IPB. Its wide textural variability can be used to elucidate the evolution of the mineralizing processes. Pyrite occurs in disseminated, massive, semi-massive, and stockwork mineralization styles. Pyrite textures include framboidal, colloform, and microcrystalline aggregates as well as idiomorphic crystals highly variable in size (Figure 5). Microscope observations reveal a textural evolution from framboidal to colloform and idiomorphic textures (Figure 5a,b), and also from porous aggregates of microcrystals to coarse idiomorphic pyrite crystals (Figure 5c–f). In stockwork mineralizations, pyrite generally occurs as coarse idiomorphic crystals (Figure 5g).

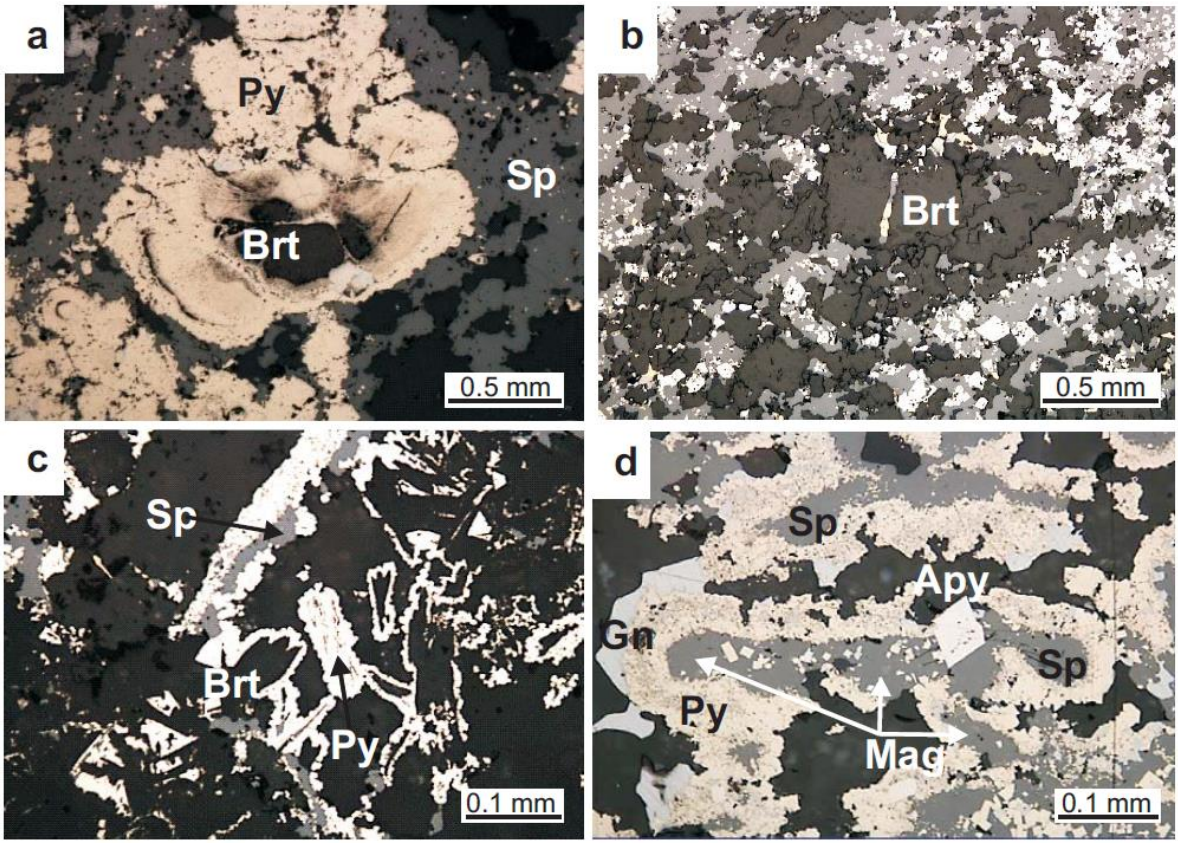

Figure 4. Optical microscope images of barite mineralizations from Magdalena deposit. (**a**) Barite (Brt) overgrown by colloform pyrite (Py), in turn, included in late sphalerite (Sp); (**b**) relicts of tabular barite crystals replaced by an association of sphalerite and fine grained pyrite; (**c**) barite laths showing pyrite rims and interstitial sphalerite; (**d**) sphalerite pseudomorph after possible barite laths rimmed by fine pyrite aggregates and galena (Gn) interstitial infillings. The idiomorphic arsenopyrite crystal (Apy) is related to a later crystallization stage.

Microcrystalline and framboidal pyrite comprise the structural framework of orebodies, and both evolved towards coarser and more idiomorphic crystals. This textural evolution was favored by an intense fracturing that promoted the circulation of hydrothermal fluids, which in turn, were involved in the remobilization and recrystallization of microcrystalline pyrite. This resulted in a banded (Figure 5e,f) and occasionally irregular (Figure 5c,d) intergrowth of inequigranular pyrite aggregates. The open microspaces generated during this recrystallization process (Figure 5f), together with a new fracturing episode (Figure 5e), increased the permeability and favored the replacement of pyrite by other sulfides (Figure 5c). In addition, aggregates of oquerous pyrite with evidence of late corrosion (Figure 5h) are also occasionally observed.

Local banded pyrite facies have been described at Tharsis [31,50] and Lousal [51]. These peculiar lithofacies shows turbidite like features having been related with tectonic instability at the sea bottom coeval with the massive sulfide deposition [48].

5.4. Polymetallic Mineralization

This mineralization was found in most of the massive sulfides of the IPB. Here, we include observations on stratiform sulfide bodies, including Magdalena, Cueva de la Mora, Aguas Teñidas, San Miguel, Aznalcóllar, Massa Valverde and Frailes, and the Frailes stockwork. As a general rule, polymetallic mineralizations tend to concentrate laterally and at the hanging wall of the deposits, although they were later redistributed by refining process associated with both the late hydrothermal activity and the Variscan deformation. This mineralization style is dominated by sphalerite and galena,

and minor chalcopyrite. These minerals partially replace and fill open spaces in pyritic orebodies. Sphalerite and galena can occur either isolated or forming intergrowth and galena filling interstices in sphalerite (Figure 6).

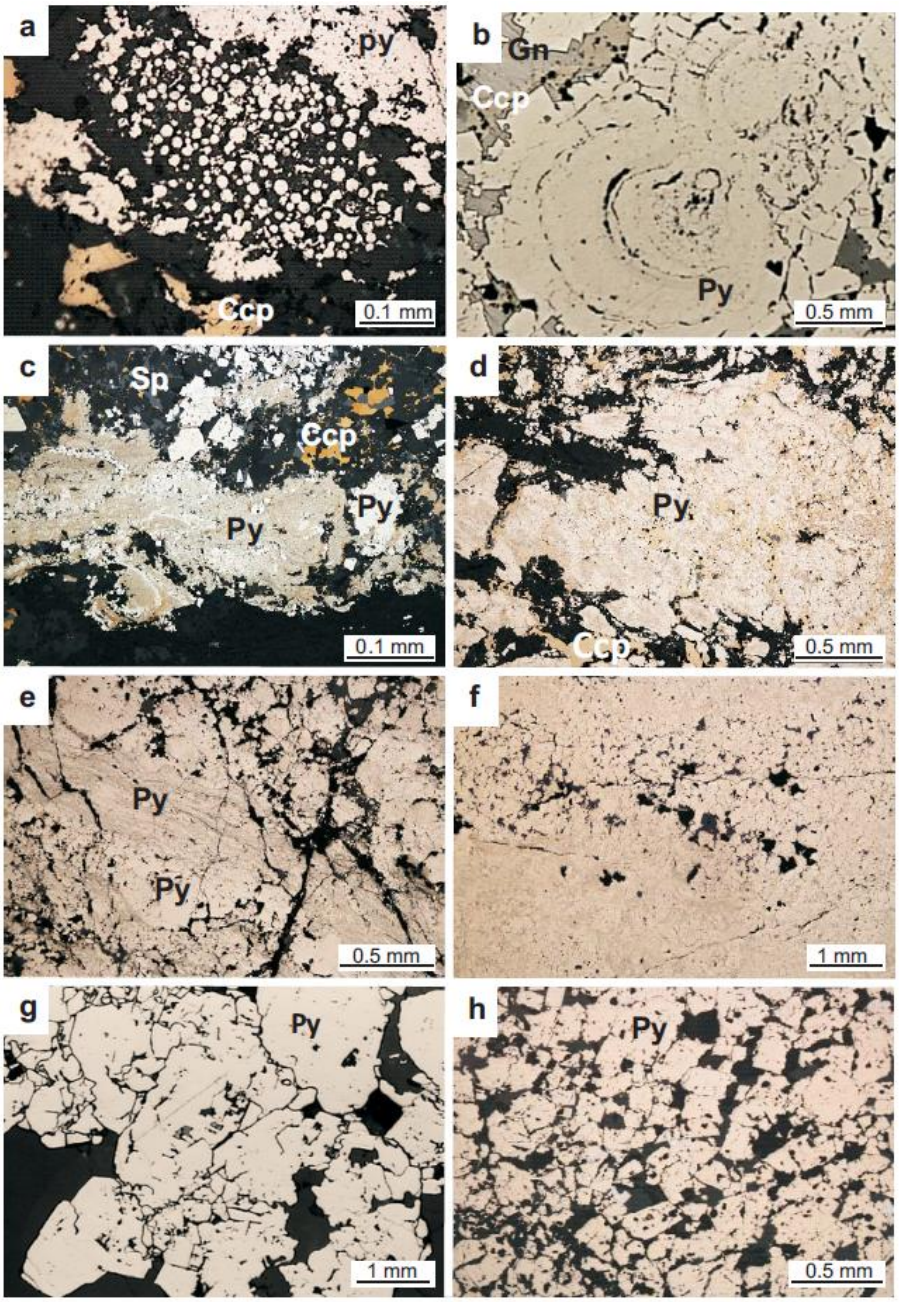

Figure 5. Optical microscope images of pyrite mineralizations from several massive sulfide deposits of the IPB. (**a**) framboidal pyrite (Py) aggregates partially recrystallized and late interstitial chalcopyrite (Ccp); (**b**) colloform pyrite nucleating over early framboids and late interstitial galena (Gn) and chalcopyrite; (**c**) very fine grained pyrite aggregates partially recrystallized and replaced by chalcopyrite and sphalerite (Sp); (**d**) porous aggregates of pyrite microcrystals partially recrystallized; (**e**) irregular banding of coarse grained pyrite and microcrystal aggregates; (**f**) massive pyrite generated by recrystallization of fine grained facies. The uneven recrystallization led to open spaces susceptible to be filled by later phases; (**g**) coarse subidiomorphic pyrite aggregates; and (**h**) oquerous pyrite showing open spaces formed by other sulfides corrosion and dissolution during distillation processes. Magdalena deposit (**a**,**c**,**d**,**h**), Aznalcóllar deposit (**b**,**g**) and Massa Valverde deposit (**f**).

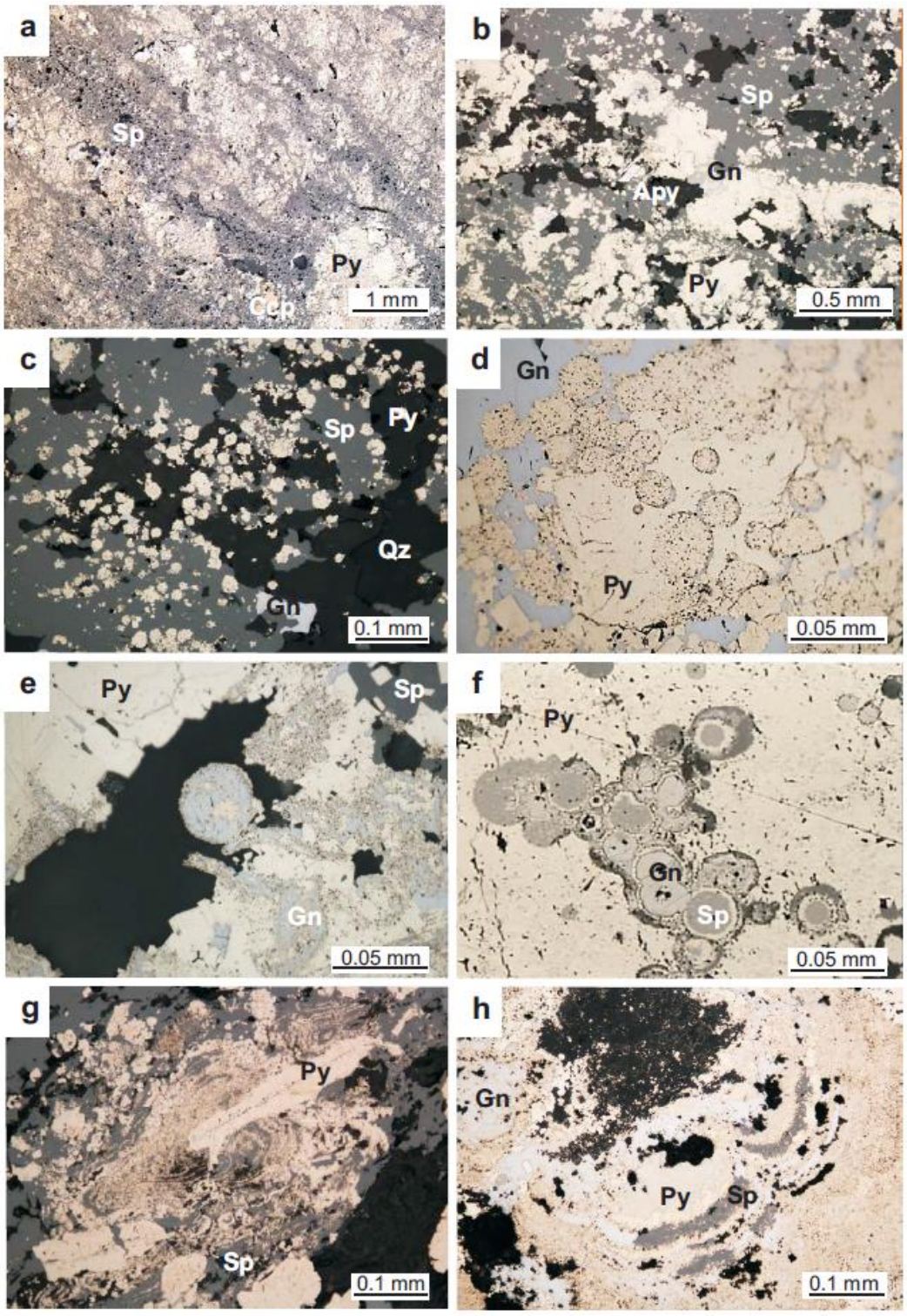

Figure 6. Optical microscope images of polymetallic mineralizations from several massive sulfide deposits of the IPB. (**a**) pyrite (Py) banded textures partially replaced by sphalerite (Sp) along high porosity bands; (**b**) advanced replacement textures on banded pyrite by polymetallic sulfide ore; (**c**) framboidal pyrite relicts partially embedded in sphalerite; (**d**) framboidal pyrite recrystallized and replaced by galena (Gn); (**e**) galena pseudomorph generated by replacement of framboidal pyrite; (**f**) aggregates of framboidal pyrite replaced by a second pyrite generation and late galena and sphalerite filling and replacing framboids and other open spaces; (**g**) selective replacement of colloform pyrite by sphalerite and galena. Massa Valverde deposit (**a**), Magdalena deposit (**b**,**c**,**g**,**h**) and Frailes deposit (**d**–**f**).

The most common texture in polymetallic mineralizations consists of an irregular banding of sphalerite and/or galena associated with pyrite (Figure 6a,b). This texture closely resembles the pyritic banded texture (compare Figure 5c,e and Figure 6a), but in these cases the most porous and permeable pyrite bands were replaced by sphalerite/galena.

Sphalerite and/or galena also replaced the hosting rocks. In some cases, these minerals include remains of the former framboidal pyrite (Figure 6c,d). In other cases, framboidal pyrite, and/or other pyrite aggregates, were indistinctly replaced by galena and/or sphalerite (Figure 6e,f). In a similar way, colloform pyrite may have been selectively replaced by sphalerite and/or galena (Figure 6g,h).

5.5. Cupriferous Mineralization

This mineralization style is commonly found in both the central and lower part of stratiform orebodies and stockworks, including deposits such as Magdalena, Cueva de la Mora, Aguas Teñidas, San Miguel, Aznalcóllar and Massa Valverde. Likely polymetallic mineralization, it was redistributed by later refining processes associated with the Variscan deformation. Cupriferous mineralizations are dominated by chalcopyrite, which filled open spaces and partially replaced earlier sulfides. However, this is not an invariable rule because chalcopyrite can also be found in different positions within the stratiform orebodies.

In cupriferous mineralizations, chalcopyrite is associated with pyrite and other major sulfides (Figure 7). The most common textural pattern is the infill of open fractures (Figure 7a), occasionally associated with the partial replacement of earlier sulfides, as occurred with microcrystalline pyrite (Figure 7b). In stockwork mineralizations, the dominant texture is the interstice infilling between idiomorphic pyrite crystals, sometimes accompanied by quartz and carbonates (Figure 7c). Similar to sphalerite and galena, chalcopyrite may also replace framboidal and colloform pyrite (Figure 7d–f). Other common textures include replacement of sphalerite by late chalcopyrite (Figure 7g) and chalcopyrite disease (Figure 7h). Both represent a progressive replacement of sphalerite by chalcopyrite by interaction of Cu-rich fluid with sphalerite.

5.6. Polymetallic Mineralization with As–Sb

This mineralization generally represents high grade zones of sulfide deposits and was identified within the stratiform sulfide bodies from Magdalena, Cueva de la Mora and Aguas Teñidas. Its irregular distribution is controlled by Variscan fractures and they are often hardly differentiable from common polymetallic and cupriferous mineralizations. They consist of pyrite, chalcopyrite, sphalerite and galena associated with late tetrahedrite–tennantite and other As and Sb sulfides and sulfosalts as minor components, such as arsenopyrite, bournonite, boulangerite, and wittichenite (Figure 8). In addition, similar mineral associations were described in stockwork mineralizations [35].

Some of their most common features are: Pb-sulfosalts (bournonite and boulangerite) generally replacing galena (Figure 8a,b); tetrahedrite–tennantite replacing both pyrite and chalcopyrite (Figure 8e); and arsenopyrite replacing pyrite and overgrowing previously formed sulfides and filling in open spaces originated by partial dissolution of colloform pyrite (Figure 8c–g). In terms of trace elements, they can include native Au, electrum, and some Bi minerals associated with small fractures (Figure 8h).

Annealing textures have been identified in these mineralizations. This pattern was observed between chalcopyrite and tetrahedrite/tennantite (Figure 9a,b); and sphalerite, chalcopyrite and tetrahedrite/tennantite (Figure 9c,d). In that case, recrystallized sphalerite exhibits characteristic lamellar twins (Figure 9c,d).

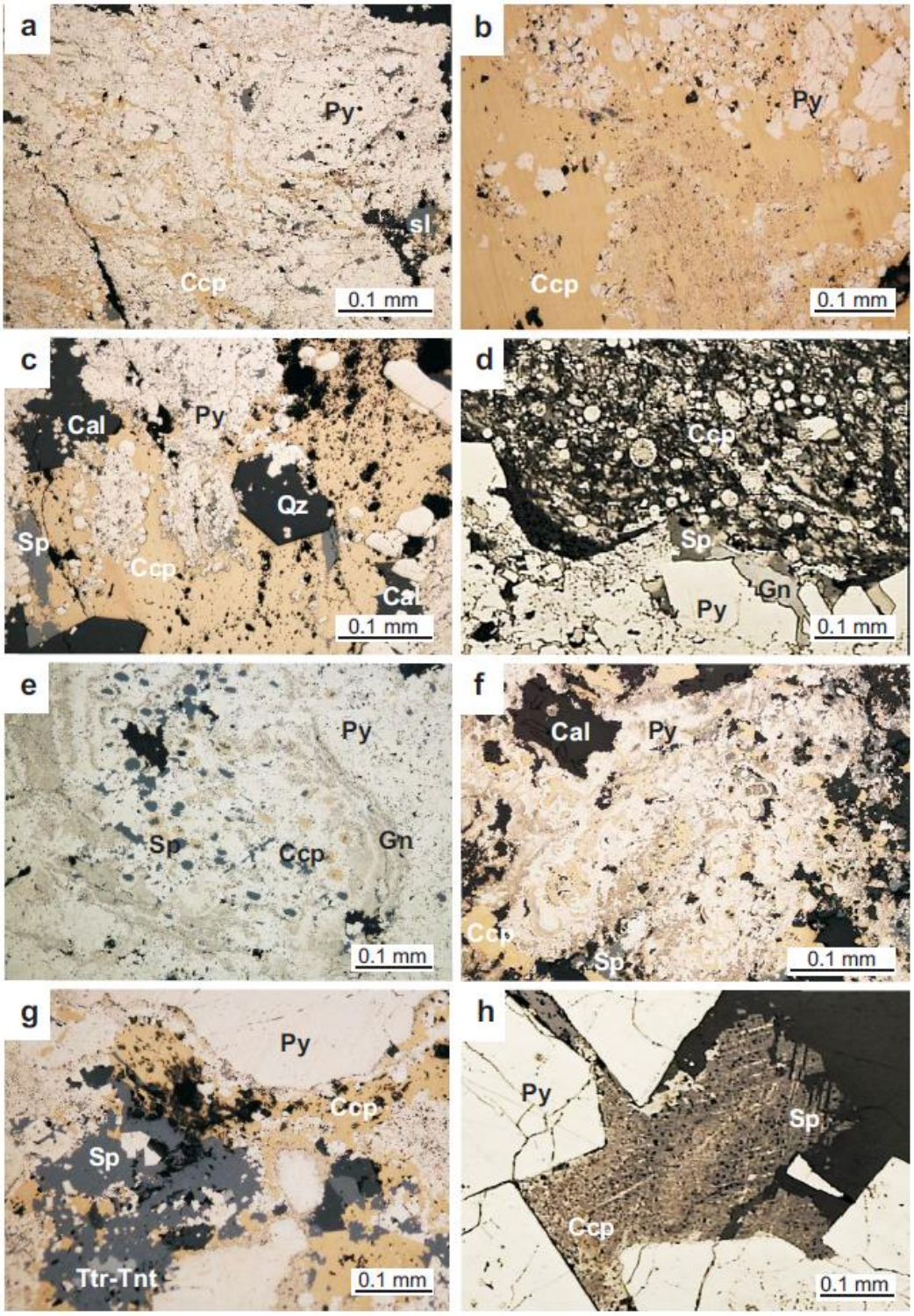

Figure 7. Optical microscope images of cupriferous mineralizations from several massive sulfide deposits of the IPB. (**a**) and (**b**) interstitial chalcopyrite (Cpp) replacing inequigranular pyrite (Py) aggregates; (**c**) replacement texture of chalcopyrite on pyrite, associated with quartz (Qz) and calcite (Cal); (**d**) pyrite framboids partially replaced by chalcopyrite; (**e**,**f**) framboidal (**e**) and colloform (**f**) primary pyrite textures replaced by chalcopyrite, sphalerite (Sp) and galena (Gn), associated with late carbonates filling open spaces; (**g**) late chalcopyrite replaced sphalerite that filled interstices in partially corroded pyrite crystals; (**h**) chalcopyrite disease on interstitial coarse grained sphalerite. Frailes deposit (**a**), Aznalcóllar deposit (**b**,**d**,**h**) and Magdalena deposit (**c**,**e**–**g**).

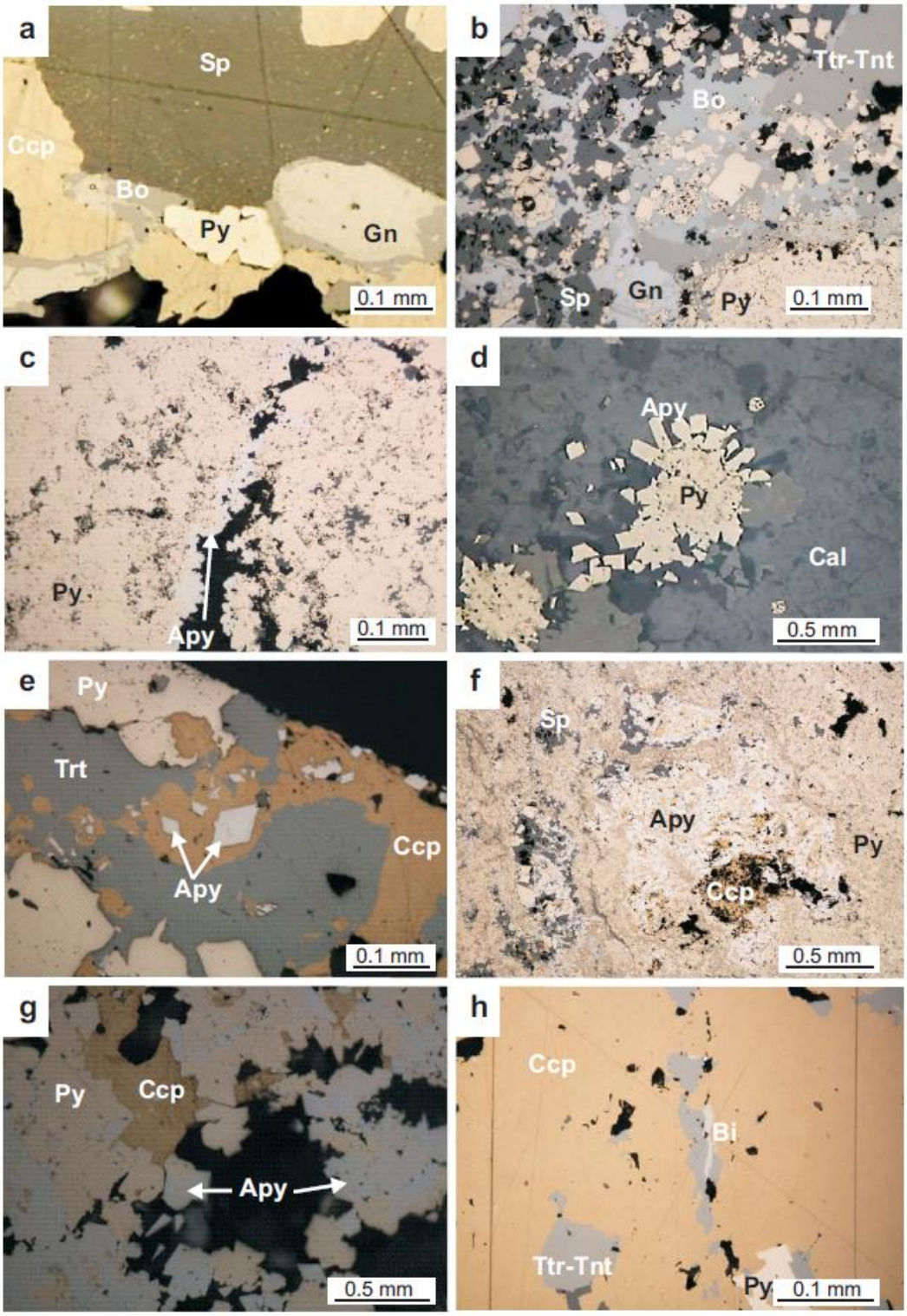

Figure 8. Optical microscope images of polymetallic mineralizations with As–Sb from several massive sulfide deposits of the IPB. (**a**,**b**) Late Cu–Pb–As–Sb sulfosalts, including boulangerite (Bo) and tetrahedrite–tennantite (Ttr–Tnt) replacing suitable sulfides; (**c**) late arsenopyrite (Apy) filling open spaces in pyrite aggregates; (**d**) fine grained pyrite overgrown by idiomorphic late arsenopyrite; (**e**) interstitial chalcopyrite (Cpp) in pyrite (Py) partially replaced by tetrahedrite–tennantite. Idiomorphic arsenopyrite crystals are also present; (**f**) arsenopyrite replacing pyrite and overgrowing former sulfides; (**g**) late arsenopyrite filling open space in a pyrite aggregates; (**h**) veinlet of bismuthine (Bi) associated with tetrahedrite–tennantite in chalcopyrite ore. Frailes deposit (**a**,**b**,**d**) and Magdalena deposit (**c**,**e**,**g**,**h**).

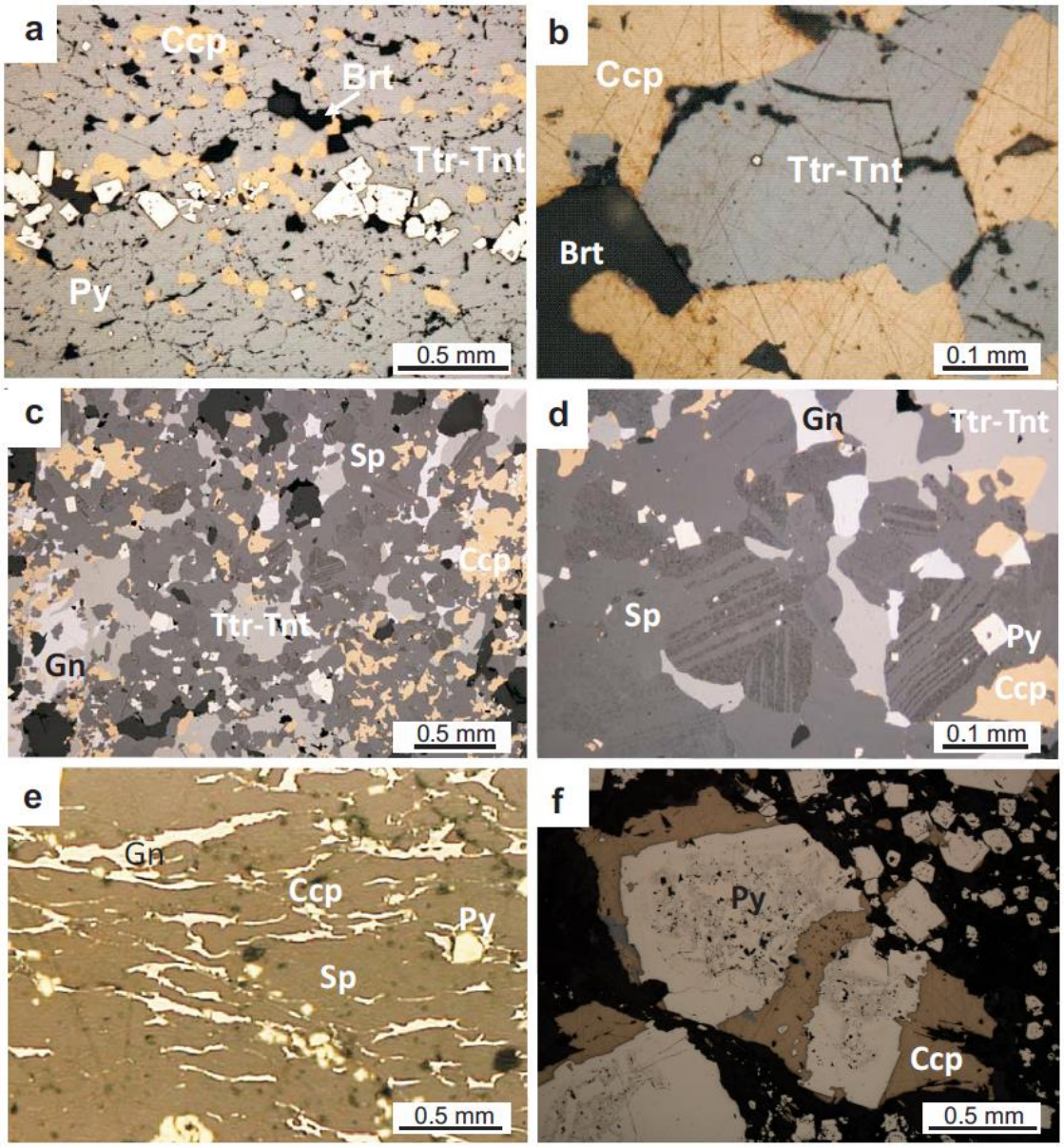

Figure 9. Optical microscope images of polymetallic mineralizations with As–Sb and deformed facies from several massive sulfide deposits of the IPB. (**a**,**b**) Annealing textures. Equigranular chalcopyrite (Ccp) and tetrahedrite (Trt) aggregates showing 120° triple junctions in grain boundaries; (**c**,**d**) sphalerite (Sp) showing lamellar twins and triple junctions; (**e**) sphalerite segregation favored by shearing deformation bands; (**f**) subidiomorphic pyrite (Py) porphyroclast showing chalcopyrite pressure shadows. Magdalena deposit (**a**–**d**,**f**) and Frailes deposit (**e**).

Deformation textures are very common at microscope scale and in local areas affected by shearing. Among them, textures with different grade of mylonitization, stretching (Figure 9e) and pressure shadows with chalcopyrite associated with pyrite (Figure 9f) are the most common.

6. Evolution of Mineralizations

The textural relationships between the major mineral components of mineralizations, as well as the spatial–temporal connection between these and the hosting rocks suggest the genetic evolution model illustrated in Figure 10.

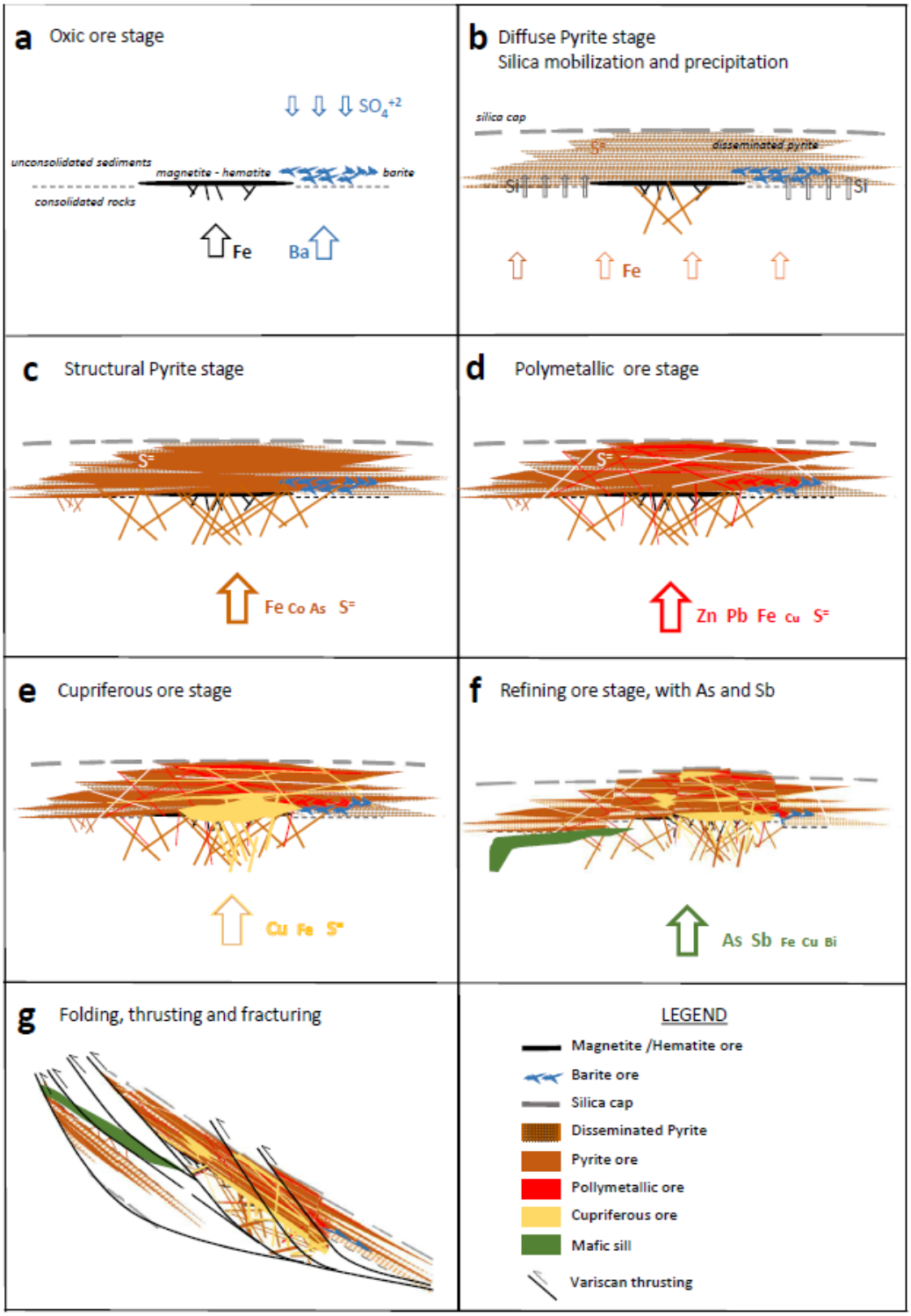

Figure 10. Seven-stage genetic model for the Iberian Pyrite Belt massive sulfides based on their mineralogical and textural evolution.

The precipitation of early magnetite and/or barite mineralizations (Figure 10a) suggests that first stages occurred characteristically near oxic conditions. This stage is mainly represented in deposits at the north of the IPB (Aguas Teñidas, Magdalena, San Miguel, Cueva de la Mora and Massa Valverde). Both magnetite and/or barite have been linked to precipitation processes from HS^--poor and slightly oxidized hydrothermal fluids [3]. Hematite–magnetite mineralizations (Figures 3 and 4) were also identified in early stages of VMS hydrothermal systems elsewhere (e.g., Kuroko, Japan, [3]).

The replacement of hematite by magnetite is favored by both a progressive rise of temperature and an evolution towards slightly reducing conditions [3].

The textural relationship between barite and sulfide minerals (Figure 4a–d) suggests a sulfate-rich early stage in which barite precipitated by a combination of marine sulfate [21,22] and Ba supplied by the hydrothermal fluids. This does not rule out the occurrence of later barite mineralizations. It simply indicates that such mineralizations were not identified in this study.

The genetic evolution model represented here (Figure 10b) includes a silica level that was identified in several deposits of the IPB (e.g., Magdalena, Cueva de la Mora, Aguas Teñidas, Aljustrel [28,29] and Tharsis [31]). Although this did not have a major influence on the mineralogical and textural evolution of the ore deposits, its genesis was essential for the evolution of mineralizations. The origin of the silica caps is related to the remobilization of silica by ascending hot fluids and its subsequent precipitation when reached to the colder sedimentary pile or the seafloor and it represents the onset of the hydrothermal activity [52–54].

The generation of sulfide mineralizations began with the precipitation of pyrite at low temperatures, leading a wide range of textures including framboidal, colloform, idiomorphic aggregates and/or microcrystalline (Figure 2b, Figure 5a–d). This first mineralization stage occurred as pyrite disseminations on the hosting volcanic rocks or organic matter rich sediments. Sulfide precipitation at this stage was favored by both the diffuse circulation of low temperature and metal-enriched hydrothermal fluids and by BSR [11,18,22,31] (Figure 10b). The progressive rise in temperature of the hydrothermal fluids evolved the increase of the vapor pressure and the focalization of hydrothermal activity. This produced hydraulic fracturation, recrystallization of previous textures, direct precipitation of idiomorphic pyrite in stockwork veins (Figure 5e–g) and infilling of open spaces of previously formed stratabound bodies (Figure 10c). As an alternative interpretation of banded pyrite lithofacies, hydraulic fracturation could induce local hoisting of the sea bottom, causing erosion and re-sedimentation of former pyrite mineralizations. The major structuration of the ore deposits took place during this mineralization stage.

The polymetallic and cupriferous ore forming stages are related to hydrothermal fluids at increasing temperature, reaching maximum temperatures during the generation of the cupriferous mineralization (Figure 10d,e) [11,18]. Precipitation of sphalerite and galena mostly occur by infilling of porous and permeable zones in the pyritic deposits, replacing often previous pyrite textures (Figures 6 and 7). In addition, sphalerite pseudomorphs after barite also suggest the interaction of hydrothermal fluids with barite (Figure 4d). Dominant textures at this stage include banded and brecciated fabrics with sphalerite and galena filling fractures and interstices within pyrite (Figure 6a,b). The relatively high solubility of Zn and Pb in the hydrothermal fluids [55,56] led to the presence of polymetallic mineralizations anywhere in the pyritic deposits, although they mainly concentrated at distal parts of sulfide bodies (Figure 10d) [11,18] (e.g., Magdalena, Cueva de la Mora, Aguas Teñidas, San Miguel, Aznalcóllar, Massa Valverde, Frailes). Due to the limited mobility of Cu and its dependence of high temperature hydrothermal fluids [56–59], Cu tended to precipitate at the core of the hydrothermal systems, either in the stockwork or at the lower part of the pyrite lenses (Figure 10e) (e.g., Magdalena, Cueva de la Mora, Aguas Teñidas, San Miguel, Aznalcóllar and Massa Valverde). However, the circulation of fluids throughout secondary porosity structures could also have favored the concentration of Cu anywhere in the orebody. This cupriferous stage was also characterized by the interaction of Cu-rich fluids with polymetallic mineralizations, allowing the replacement of sphalerite by chalcopyrite (Figure 7g) and mobilizing Zn to more distal areas. Most of the genetic models dealing with VMS-type deposits agree with an evolution to rising temperature until the generation of the high temperature cupriferous and pyritic mineralizations [1–3]. In the IPB hydrothermal systems, the temperature decreased after the generation of the cupriferous mineralization until the system became inactive.

The polymetallic mineralizations with As–Sb within the massive bodies seem to be related with the reactivation of the hydrothermal systems linked to the emplacement of basic to intermediate sills (Figure 10f). In some IPB deposits, such as Magdalena, Aguas Teñidas, or Cueva de la Mora, both

these sills and polymetallic mineralizations with As–Sb were identified, suggesting a relationship between them. They postdate the major mineralization stages as evidenced by the lack of hydrothermal alteration typically characterizing the footwall of VMS systems. However, sills are sheared and deformed indicating that they predate the Variscan folding. The sills' emplacement resulted in a local increase of temperature that favored the liberation of As- and Sb-bearing hydrothermal fluids throughout Variscan fractures. In that sense, German et al. [60] reported late Variscan veins of stibnite and arsenopyrite in the central IPB. These interacted with early mineralizations promoting annealing textures, including equigranular aggregates of chalcopyrite and tetrahedrite with triple points (Figure 9a,b), or sphalerite showing lamellar twins (Figure 9c,d). Similar textures were described in both Pribran (Czech Republic) and Austinville (WV, USA) deposits being related to thermal stress [61,62].

The interaction between these late hydrothermal fluids and sulfide mineralizations led to multiple effects. Among them, the remobilization mainly of Cu at the lower part of orebodies promoted a textural pattern characterized by pore-rich massive pyrite bodies as evidence of metal distillation processes (Figure 5h). The leached Cu was transported and redeposited in other areas as tetrahedrite–tennantite and minor chalcopyrite. Often, this process involves the formation of arsenopyrite and As–Sb sulfosalts, partially replacing early pyrite, sphalerite, and galena (Figure 8). Occasionally, the local increase of temperature produced recrystallization or annealing of all sulfides except pyrite. This mechanism could explain the occurrence of high-grade refining zones in Magdalena, Cueva de la Mora, and Aguas Teñidas. The hydrothermal fluid can also be diffused by capillarity throughout the sulfide mineralizations. This favored the occurrence of zones of arsenopyrite dissemination as infillings of open spaces or replacement of early sulfides (Figure 8c–g).

Last stage in the evolution of mineralizations relates to the textural evolution associated with folding and thrusting during the Variscan orogeny (Figure 10g). At this stage, remobilizations controlled by differential viscoelastic behavior of metallic sulfides took place in the ore deposits promoting local metal enrichments. For example, Cu enrichment associated with this mechanism was observed in Aguas Teñidas and Magdalena (Figure 9e,f). In addition, in Neves Corvo, the so-called Rubanée mineralization represents an exceptional concentration of Cu, as chalcopyrite, in a sheared zone along a stockwork type mineralization [46]. In a similar way, there are also "ore shoots" of polymetallic mineralizations associated with the selective remobilization of galena, sphalerite, and/or tetrahedrite–tennantite, which were disseminated early in pyritic deposits. In this case, the dominant texture consists of a rough shear-banding defined by both the stretching of ductile minerals (i.e., galena and sphalerite) and pyrite, as rigid porphyroclast, surrounded by foliation (Figure 9e,f). Moreover, Castroviejo et al. [25] also reported post-depositional tectonic modification of VMS deposits in the IPB and Marignac et al. [33] described metal remobilization during the Variscan metamorphism.

7. Conclusions

The mineral composition of massive sulfide deposits from the IPB mostly comprises of pyrite, and subordinate sphalerite, galena, chalcopyrite, arsenopyrite, tetrahedrite–tennantite, cobaltite, Sb–As–Bi sulphosalts, gold, and electrum. Common oxidized phases include magnetite, hematite, cassiterite, and barite.

These minerals show a wide range of textures, including corrosion, dissolution–replacement, colloform, framboids, intergrowths, overgrowths, filling interstices, microcrystalline, banded, recrystallization, euhedral aggregates and annealing.

Textural relationships between minerals is intricate. Oxidized phases appear partial or totally replaced by pyrite. Pyrite texture evolves from fine framboids to colloform and coarser euhedral aggregates, whereas sphalerite, galena, and chalcopyrite appear mainly to fill open spaces in pyrite aggregates. Sb and As sulfides and sulfosalts appear in a later stage of the mineral precipitation sequence, showing annealing textures and overgrowth and replacement of early sulfides.

The mineralogical and textural evolution of massive sulfides presented here leads to a common general model for IPB deposits including four main stages: (1) A previous oxic system dominated by

Fe-oxides and barite precipitation; (2) BSR disoxic dominated conditions; and (3) a high temperature hydrothermal system responsible for main base metal mineralization. Later in this stage, the refining processes took place, driven by the emplacement of mafic magmas at depth leading the Sb- and As-rich mineralization; and (4) formation of ore shoots by selective remobilization during the Variscan deformation.

Author Contributions: For research articles with several authors, a short paragraph specifying their individual contributions must be provided. The following statements should be used "conceptualization: G.R.A. and L.Y.; methodology: all; validation: all; formal analysis: all; investigation: all; resources: all; writing—original draft preparation, G.R.A., L.Y. F.G. and R.S.; writing—review and editing: all; supervision: all; project administration: R.S.; funding acquisition: R.S.".

Funding: This research is a contribution to projects MOS (grant number CGL2016-79204-R), which are supported by the Spanish Government.

Acknowledgments: The authors thank all mining companies operating in the IPB for the field assistance and the ongoing collaboration and anonymous referees for their reviews which have greatly helped to improve this paper.

Conflicts of Interest: The authors declare no conflict of interest.

References

1. Lydon, J.W. Ore deposit models, 14, volcanogenic massive sulphide deposits Part 2: Genetic models. *Geosci. Can.* **1988**, *15*, 43–65.
2. Large, R.R. Australian volcanic-hosted massive sulfide deposits: Features, styles, and genetic models. *Econ. Geol.* **1992**, *87*, 471–510. [CrossRef]
3. Ohmoto, H. Formation of volcanogenic massive sulfide deposits: The Kuroko perspective. *Ore Geol. Rev.* **1996**, *10*, 135–177. [CrossRef]
4. Franklin, J.M.; Gibson, H.L.; Galley, A.G.; Jonasson, I.R. Volcanogenic massive sulfide deposits. In *Economic Geology 100th Anniversary Volume*; Hedenquist, J.W., Thompson, J.F.H., Goldfarb, R.J., Richards, J.P., Eds.; Economic Geology: New Haven, CT, USA, 2005; pp. 523–560.
5. Tornos, F.; Peter, J.M.; Allen, F.; Conde, C. Controls on the siting and style of volcanogenic massive sulphide deposits. *Ore Geol. Rev.* **2015**, *68*, 142–163. [CrossRef]
6. Eldridge, C.S.; Barton, P.B.; Ohmoto, H. Mineral textures and their bearing on formation of the Kuroko orebodies. In *Economic Geology, Monograph 5*; Ohmoto, H., Skinner, B.J., Eds.; Economic Geology: New Haven, CT, USA, 1983; pp. 241–281.
7. Gibson, H.L.; Allen, R.L.; Riverin, G.; Lane, T.E. The VMS model: Advances and application to exploration targeting. In Proceedings of the Fifth Decennial International Conference on Mineral Exploration, Toronto, ON, Canada, 9–12 September 2007; Available online: http://www.dmec.ca/ex07-dvd/E07/pdfs/49.pdf (accessed on 22 October 2019).
8. Pinedo Vara, I. *Piritas de Huelva. Su Historia, Minería y Aprovechamiento*; Summa: Madrid, Spain, 1963; p. 1003.
9. Nocete, F.; Álex, E.; Nieto, J.M.; Sáez, R.; Bayona, M.R. An archaeological approach to regional environmental pollution in the South-Western Iberian Peninsula related to Third Millennium BC mining and metallurgy. *J. Archaeol. Sci.* **2005**, *32*, 1566–1576. [CrossRef]
10. Sáez, R.; Almodóvar, G.R.; Pascual, E. Geological constraints on massive sulphide genesis in the Iberian Pyrite Belt. *Ore Geol. Rev.* **1996**, *11*, 429–452. [CrossRef]
11. Sáez, R.; Pascual, E.; Toscano, M.; Almodóvar, G.R. The Iberian type of volcano-sedimentary massive sulphide deposits. *Miner. Depos.* **1999**, *34*, 549–570. [CrossRef]
12. Leistel, J.M.; Marcoux, E.; Thiéblemont, D.; Quesada, C.; Sánchez, A.; Almodóvar, G.R.; Pascual, E.; Sáez, R. The volcanic-hosted massive sulphide deposits of the Iberian Pyrite Belt, Review and preface to the Thematic Issue. *Miner. Depos.* **1998**, *33*, 2–30. [CrossRef]
13. Martin-Izard, A.; Arias, D.M.; Arias, M.; Gumiel, P.; Sanderson, D.J.; Castañón, C.; Lavandeira, A.; Sánchez, J. A new 3D geological model and interpretation of structural evolution of the world-class Rio Tinto VMS deposit, Iberian Pyrite Belt (Spain). *Ore Geol. Rev.* **2015**, *71*, 457–476. [CrossRef]
14. Relvas, J.M.R.S.; Tassinari, C.C.G.; Munhá, J.; Barriga, F.J.A.S. Multiple sources for ore-forming fluids in the Neves Corvo VHMS deposit of the Iberian Pyrite Belt (Portugal): Strontium, neodymium and lead isotope evidence. *Miner. Depos.* **2001**, *36*, 416–427. [CrossRef]

15. Schermerhorn, L.J.G. An outline stratigraphy of the Iberian Pyrite Belt. Bolet. *Geol. Min.* **1971**, *82*, 239–268.
16. Barriga, F.J.A.S. Metallogenesis in the Iberian Pyrite Belt. In *Pre-Mesozoic Geology of Iberia*; Dallmeyer, R.D., Martínez-García, E., Eds.; Springer: Berlin/Heidelberg, Germany, 1990; pp. 369–379.
17. Almodóvar, G.R.; Sáez, R.; Toscano, M.; Pascual, E. Co-Ni and "inmobile" element behaviour in ancient hydrothermal systems, Aznalcóllar, Iberian Pyrite Belt, Spain. In *Mineral Deposits: From Their Origin to Their Environmental Impacts*; Pašava, J., Kríbek, R., Zák, K., Eds.; Balkema: Roterdam, The Netherlands, 1995; pp. 217–220.
18. Almodóvar, G.R.; Sáez, R.; Pons, J.M.; Maestre, A.; Toscano, M.; Pascual, E. Geology and genesis of the Aznalcóllar massive sulphide deposits, Iberian Pyrite Belt, Spain. *Miner. Depos.* **1998**, *33*, 111–136. [CrossRef]
19. Almodóvar, G.R.; Sáez, R. Los sulfuros masivos de la Faja Pirítica Ibérica. In *Geología de España*; Vera, J.A., Ed.; Sociedad Geológica de España—Instituto Geológico y Minero de España: Madrid, Spain, 2004; pp. 207–209.
20. Tornos, F.; Solomon, M.; Conde, C.; Spiro, B.F. Formation of the Tharsis massive sulfide deposit, Iberian Pyrite Belt: Geological, lithogeochemical, and stable isotope evidence for deposition in a brine pool. *Econ. Geol.* **2008**, *103*, 185–214. [CrossRef]
21. Velasco, F.; Sánchez-España, J.; Boyce, A.J.; Fallick, A.E.; Sáez, R.; Almodóvar, G.R. A new sulphur isotopic study of some Iberian Pyrite Belt deposits: Evidence of a textural control on sulphur isotope composition. *Miner. Depos.* **1998**, *34*, 4–18. [CrossRef]
22. Inverno, C.M.; Solomon, M.; Barton, M.D.; Foden, J. The Cu stockwork and massive sulfide ore of the Feitais volcanic-hosted massive sulfide deposit, Aljustrel, Iberian Pyrite Belt, Portugal: A mineralogical, fluid inclusion, and isotopic investigation. *Econ. Geol.* **2008**, *103*, 241–267. [CrossRef]
23. Sáez, R.; Moreno, C.; González, F. Synchronous deposition of massive sulphide deposits in the Iberian Pyrite Belt: New data from Las Herrerías and La Torerera ore-bodies. *Comptes Rendus Geosci.* **2008**, *340*, 829–839. [CrossRef]
24. Martin-Izard, A.; Arias, D.M.; Arias, M.; Gumiel, P.; Sanderson, D.J.; Castañón, C.; Sánchez, J. Ore deposit types and tectonic evolution of the Iberian Pyrite Belt: From transtensional basins and magmatism to transpression and inversion tectonics. *Ore Geol. Rev.* **2016**, *79*, 254–267. [CrossRef]
25. Castroviejo, R.; Quesada, C.; Soler, M. Post-depositional tectonic modification of VMS deposits in Iberia and its economic significance. *Miner. Depos.* **2011**, *46*, 615–637. [CrossRef]
26. Yesares, L.; Sáez, R.; Nieto, J.M.; Almodóvar, G.R.; Gómez, C.; Escobar, J.M. The Las Cruces deposit, Iberian Pyrite Belt, Spain. *Ore Geol. Rev.* **2015**, *66*, 25–46. [CrossRef]
27. Moreno, C.; Sierra, S.; Saéz, R. Evidence for catastrophism at the Famennian–Dinantian boundary in the Iberian Pyrite Belt. In *Recent Advances in Lower Carboniferous Geology*; Strogen, P., Sommerville, I.D., Jones, J.L., Eds.; The Geological Society: London, UK, 1996; pp. 153–162.
28. Barriga, F.J.A.S. Hydrothermal Metamorphism and Ore Genesis at Aljustrel, Portugal. Ph.D. Thesis, University of Western Ontario, London, ON, Canada, 1983; p. 386, Unpublished.
29. Barriga, F.J.A.S.; Fyfe, W.S. Giant pyritic base-metal deposits: The example of Feitais (Aljustrel, Portugal). *Chem. Geol.* **1988**, *69*, 331–343. [CrossRef]
30. Marcoux, E. Lead isotope systematics of the giant massive sulphide deposits in the Iberian Pyrite Belt. *Miner. Depos.* **1998**, *33*, 45–58. [CrossRef]
31. Sáez, R.; Moreno, C.; González, F.; Almodóvar, G.R. Black shale and massive sulfide deposits: Causal or casual relationships? Insights from Rammelsberg, Tharsis, and Draa Sfar. *Miner. Depos.* **2011**, *46*, 585–614. [CrossRef]
32. Tornos, F.; Heinrich, C.A. Shale basins, sulfur-deficient ore brines and the formation of exhalative base metal deposits. *Chem. Geol.* **2008**, *247*, 195–207. [CrossRef]
33. Marignac, C.; Diagana, B.; Cathelineau, M.; Boiron, M.C.; Banks, D.; Fourcade, S.; Vallance, J. Remobilisation of base metals and gold by Variscan metamorphic fluids in the south Iberian Pyrite Belt: Evidence from the Tharsis VMS deposit. *Chem. Geol.* **2003**, *194*, 143–165. [CrossRef]
34. De Miguel, J.M.G. Mineralogía, paragénesis y sucesión de los sulfuros masivos en la Faja Pirítica en el suroeste de la Península Ibérica. *Bol. Geol. Min.* **1990**, *101*, 73–105.
35. Marcoux, E.; Moelo, Y.; Leistel, J.M. Compared ore mineralogy and geochemistry of the massive sulfide and stringer ore deposits of the Southern Spain. *Miner. Depos.* **1996**, *31*, 1–26.
36. Gaspar, O.C. Mineralogy and sulfide mineral chemistry of the Neves–Corvo ores, Portugal: Insight into their genesis. *Can. Mineral.* **2002**, *40*, 611–636. [CrossRef]

37. Oliveira, D.P.S.; Matos, J.X.M.; Rosa, C.J.P.; Rosa, D.R.N.; Figueiredo, M.O.; Silva, T.P.; Guimarães, F.; Carvalho, J.R.S.; Pinto, Á.M.M.; Relvas, J.R.M.S.; et al. The Lagoa Salgada Orebody, Iberian Pyrite Belt. *Econ. Geol.* **2011**, *106*, 1111–1128. [CrossRef]
38. Saéz, R. La Faja Pirítica Ibérica. Una Perspectiva Geológica, Arqueológica y Ambiental. Ph.D. Thesis, University of Huelva, Huelva, Spain, 2010. Unpublished.
39. González, F.; Moreno, C.; Sáez, R.; Clayton, G. Ore genesis age of the Tharsis Mining District (Iberian Pyrite Belt): A palynological approach. *J. Geol. Soc.* **2002**, *159*, 229–232. [CrossRef]
40. Barrie, C.T.; Amelin, Y.; Pascual, E. U–Pb geochronology of VMS mineralization in the Iberian Pyrite Belt. *Miner. Depos.* **2002**, *37*, 684–703. [CrossRef]
41. Silva, J.B.; Oliveira, J.T.; Ribeiro, A. South Portuguese zone. Structural outline. In *Pre-Mesozoic Geology of Iberia*; Dallmeyer, R.D., García, E.M., Eds.; Springer: Berlin/Heidelberg, Germany, 1990; pp. 348–362. ISBN 13:978-3-642-83982-5.
42. Pereira, Z.; Sáez, R.; Pons, J.M.; Oliveira, J.T.; Moreno, C. Edad devónica (Struniense) de las mineralizaciones de Aznalcóllar (Faja Pirítica Ibérica) en base a palinología. *Geogaceta* **1996**, *20*, 1609–1612.
43. Simancas, J.F. Geología de la Extremidad Oriental de la Zona Surportuguesa. Ph.D. Thesis, University of Granada, Granada, Spain, 1983. Unpublished.
44. Simancas, J.F.; Carbonell, R.; Lodeiro, F.G.; Estaún, A.P.; Juhlin, C.; Ayarza, P.; Kashubin, A.; Azor, A.; Poyatos, D.M.; Almodóvar, G.R.; et al. The crustal structure of the transpressional Variscan orogen of SW Iberia: The IBERSEIS deep seismic reflection profile. *Tectonics* **2003**, *22*, 1063–1078. [CrossRef]
45. Almodóvar, G.R.; Sáez, R.; Toscano, M.; Moreno, C.; Donaire, T.; Nieto, J.M.; González, F.; Yesares, M.D.; Pascual, E. Hidrotermalismo de hace más de 350 millones de años: La Faja Pirítica Ibérica. *Rev. Enseñanza Cienc. Tierra* **2012**, *20*, 210–213.
46. Relvas, J.M.R.S.; Barriga, F.J.A.S.; Ferreira, A.; Noiva, P.C.; Pacheco, N.; Barriga, G. Hydrothermal alteration and mineralization in the Neves-Corvo volcanic-hosted massive sulfide deposit, Portugal. I. Geology, mineralogy, and geochemistry. *Econ. Geol.* **2006**, *101*, 753–790. [CrossRef]
47. Leistel, J.M.; Marcoux, E.; Deschamps, I. Chert in the Iberian Pyrite Belt. *Miner. Depos.* **1998**, *33*, 59–81. [CrossRef]
48. Tornos, F. Environment of formation and styles of volcanogenic massive sulphides: The Iberian Pyrite Belt. *Ore Geol. Rev.* **2006**, *28*, 259–307. [CrossRef]
49. Boulter, C.A. Río Tinto-Guaymas comparisons: Super-giant mineralization in an ancient sill-sediment complex. *Geology* **1994**, *21*, 801–804. [CrossRef]
50. Strauss, G.K.; Madel, J. Geology of massive sulphide deposits in the Spanish Portuguese Pyrite Belt. *Geol. Rundsch.* **1974**, *63*, 191–211. [CrossRef]
51. Strauss, G.K. *Sobre la Geología de la Provincia Piritífera del Suroeste de la Península Ibérica y de sus Yacimientos, en Especial Sobre la Mina de Pirita de Lousal*; Instituto Geológico y Minero de España: Madrid, Spain, 1971; p. 266. (In Spanish)
52. Barnes, H.L. *Geochemistry of Hydrothermal Ore Deposits*, 2nd ed.; John Wiley & Sons: New York, NY, USA, 1979.
53. Fournier, R.O. The behavior of silica in hydrothermal solutions. In *Geology and Geochemistry of Epithermal Systems*; Berger, B.R., Bethke, P.M., Eds.; The Society of Economic Geologists: Littleton, CO, USA, 1986; pp. 45–62.
54. Brown, K. Thermodynamics and kinetics of silica scaling. In Proceedings of the International Workshop on Mineral Scaling, Manila, Philippines, 25–27 May 2011.
55. Crerar, D.A.; Barnes, H.L. Ore solution chemistry V. Solubilities of chalcopyrite assemblages in hydrothermal solution at 200 to 350 °C. *Econ. Geol.* **1976**, *71*, 772–794. [CrossRef]
56. Seward, T.M.; Williams-Jones, A.E.; Migdisov, A.A. The chemistry of metal transport and deposition by ore-forming hydrothermal fluids. In *Treatise on Geochemistry*, 2nd ed.; Holland, H.D., Turekian, K.K., Eds.; Elsevier-Pergamon: Amsterdam, The Netherland, 2014; Volume 13.
57. Seewald, J.S.; Seyfried, W.E. The effect of temperature on metal mobility in subseafloor hydrothermal systems: Constraints from basalt alteration experiments. *Earth Planet. Sci. Lett.* **1990**, *101*, 388–403. [CrossRef]
58. Xiao, Z.; Gammons, C.H.; Williams-Jones, A.E. Experimental study of copper (I) chloride complexing in hydrothermal solutions at 40 to 300 °C and saturated water vapour pressure. *Geochim. Cosmochim. Acta* **1998**, *62*, 2949–2964. [CrossRef]

59. Solomon, M.; Walshe, J.L. The formation of massive sulfide deposits on the sea floor. *Econ. Geol.* **1979**, *74*, 797–813. [CrossRef]
60. German, K.; Volker, L.; Banks, D.A.; Simon, K.; Hoefs, J. Late Hercynian polymetallic vein-type base-metal mineralization in the Iberian Pyrite Belt: Fluid-inclusion and stable-isotope geochemistry (S–O–H–Cl). *Miner. Depos.* **2003**, *38*, 953–967. [CrossRef]
61. Fleet, M.E. Structural transitions in natural ZnS. *Am. Mineral.* **1977**, *62*, 540–546.
62. Akizuki, M. Investigation of phase transition of natural ZnS minerals by high resolution electron microscopy. *Am. Mineral.* **1981**, *66*, 1006–1012.